

Low-loss planar components for THz wireless communications

Hichem Guerboukha, Kathirvel Nallappan, Yang Cao, and Maksim Skorobogatiy

Polytechnique Montreal, Montreal (QC), Canada, H3C 3A7

Corresponding authors: hichem.guerboukha@polymtl.ca, maksim.skorobogatiy@polymtl.ca

Abstract — Shifting the carrier frequency to the terahertz range is seen by many as a potential way to increase the bandwidth in wireless communications. However, losses in conventional dielectrics become important when increasing the frequency. When introducing low-RI, low-loss subwavelength inclusions in a solid material, we can reduce the overall losses, opening a way to create optical components even with lossy material. In this work, we present low-loss planar porous THz components. We design, fabricate and characterize planar lenses and orbital angular momentum phase plates.

Index Terms — Wireless communications, terahertz, beam forming, lens, orbital angular momentum.

I. INTRODUCTION

Taming the terahertz (THz) waves is considered as the next frontier in wireless communications. To meet the ever-increasing wireless communications bandwidth requirements, shifting the carrier frequency toward the THz range (from 100 GHz to 10 THz) is seen by many as the next frontier in wireless communications [1]. Recently, transmission of data at distance greater than 2 km with data

rates of 10 Gbps (amplitude shift keying) and 20 Gbps (quadrature phase shift keying) were reported [2,3].

To enable THz communications, THz components for beam forming are necessary [4-6]. One major problem when shifting to higher frequencies is the higher losses in conventional materials. Since air remain the material with the lowest absorption losses, porous devices have been proposed in the past to increase the fraction of energy interacting with air [7]. When introducing low-refractive index (RI), low loss, subwavelength inclusions, the real part of the effective material RI reduces significantly slower than its absorption losses. Thus, by introducing porosity into optical materials, one can create optical components that would have identical performance characteristic as their non-porous counterparts, while having overall much lower absorption losses that scale as $\sim 1/n_m^2$ with the base material refractive index.

In this work, we design, fabricate and characterize two planar components for THz beam forming: 1) planar lens and 2) orbital angular moment phase plate. Lenses are essential in many optical systems to collimate and focus the

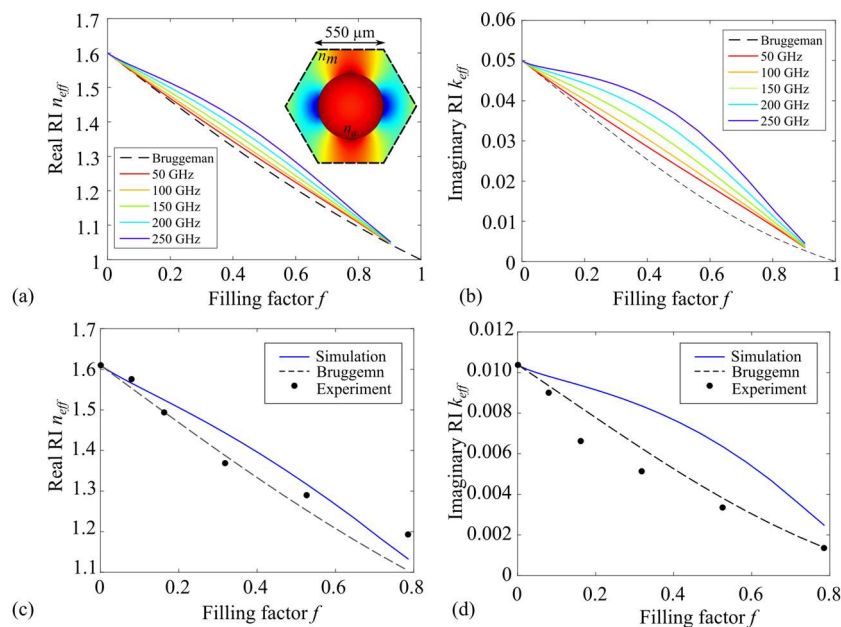


Fig. 1. (a) Real and (b) imaginary parts of the refractive index at different frequencies calculated theoretically using the Bruggeman model (dotted line) and numerically (color lines) as a function of the filling factor ($\tilde{n}_m = 1.6 + 0.05i$). The inset in (a) shows a typical fundamental mode obtained numerically and the geometry of the cell unit used in the numerical calculations. (c) Real and (d) imaginary parts of the refractive index calculated theoretically using the Bruggeman model (dotted line) and numerically (blue line) compared to the experimental results (black dots) at a frequency of 150 GHz.

THz beam. Over regular lenses, porous planar lenses allow for higher transmission ratios and more compact system designs [8]. Orbital angular momentum (OAM) is a well-established property of light that manifest itself as a helical wavefront with azimuthal phase term. In communications, OAM states are explored as an additional spatial division multiplexing (SDM) technique [9].

This paper is structured as follows. First, in Section II, we present the cell unit simulations necessary to design various planar components. Then, in Section III and Section IV, we fabricate and characterize planar lens and orbital angular momentum phase plate respectively.

II. DESIGN AND FABRICATION OF THE LOW-LOSS THZ COMPONENTS

The planar components are designed with gradient-index distributions. They are made of circular holes of refractive index n_a (air) in a host material with refractive index n_m (inset of Fig. 1a). When the hole diameter is smaller than the wavelength, the radiation will “see” an effective refractive index n_{eff} whose value is bounded between n_a and n_m . We assume that the inclusions are made of air and present no losses:

$$\varepsilon_a = n_a^2 = 1 \quad (1)$$

while the host material power absorption losses α_m are included in the imaginary part of its refractive index:

$$\varepsilon_m = (n_m + ik_m)^2 = \left(n_m + i\alpha_m \frac{\lambda}{4\pi}\right)^2 \quad (2)$$

with ε_a and ε_m the complex permittivities of the air and the material respectively. Using Bruggeman model [10], we express the transverse component of the effective permittivity as:

$$\varepsilon_{eff} = \sqrt{\left(\frac{1}{2} - f\right)^2 (\varepsilon_a - \varepsilon_m)^2 + \varepsilon_a \varepsilon_m - \left(\frac{1}{2} - f\right) (\varepsilon_a - \varepsilon_m)} \quad (3)$$

Using COMSOL software, we solve for the fundamental mode of a hexagonal cell unit (lattice length of $550 \mu\text{m}$) with periodic boundaries to find the real part (Fig. 1a) and imaginary (Fig. 1b) effective refractive index as a function of the fill factor. We confirm that the numerical simulations approach the Bruggeman results when the wavelength is larger than the cell dimensions.

Next, to fabricate planar components, we use a laser cutting in our local Fablab to make holes with varying diameters in a plate of acrylic (PMMA) of refractive index $n_m = 1.61$. Then, using THz time-domain spectroscopy, we extract the refractive index at 0.15 THz using the standard procedure explained in [11]. The measured refractive indices for different hole diameters are comparable to the simulations and the Bruggeman model as it can be seen in Fig. 1c and 1d (circles compared to line).

In the following section, we use the results of Fig. 1b to design and fabricate a planar lens and an OAM phase plate. To characterize the planar components, we perform THz imaging using a modified THz time-domain spectroscopy system. A Ti:Sapphire laser (100 fs, 800 nm, 100 MHz) delivers 300 mW and 10 mW to the THz photoconductive

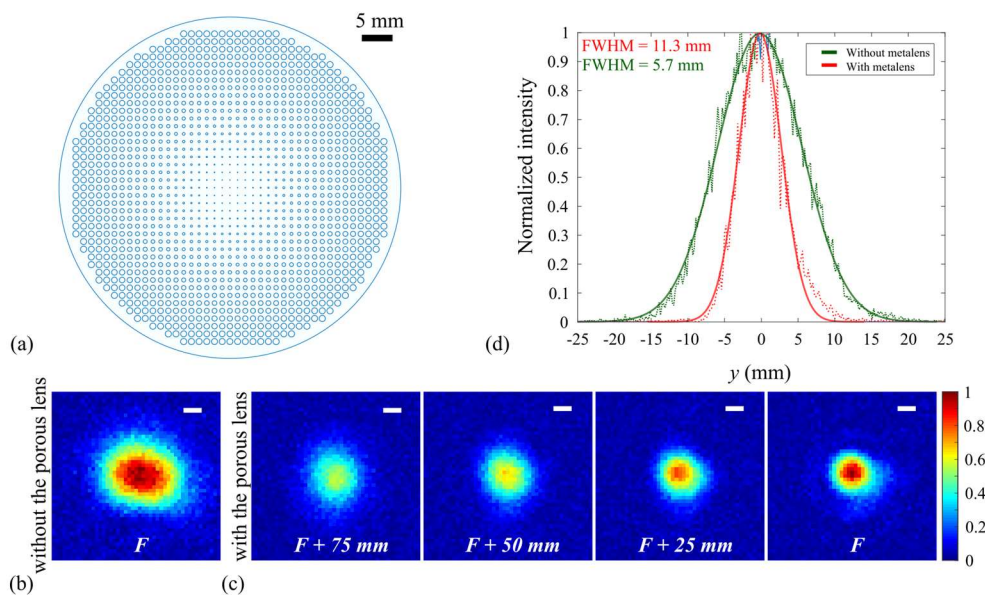


Fig. 2. (a) Design of the planar lens with the diameter of the holes varying as a function of the radius following Eq. 1. (b) THz image at 0.2 THz without the planar lens and (c) with the planar lens at various focal positions. (d) Cross-sections of the intensity of the THz beam at the focal plane with (red) and without (green) the planar lens.

emitter and antenna respectively. On the emitter side, a linear delay line is placed prior to a high-power interdigitated antenna supplied with 15 V at 5 kHz. In the detection side, we use a fiber-coupled detector to allow convenient scanning of the image plane. The optical beam is focused into a polarization-maintaining optical fiber with the input end fixed on the optical table, while the output end is placed on a 3D micropositioning stage for imaging. To compensate for the positive group-velocity dispersion in the optical fiber, a dispersion pre-compensation system made of two diffraction gratings and a mirror is used to add negative dispersion in the optical beam. See [12] for more details about the experimental setup. The THz imaging system allows to obtain both amplitude and phase of the THz radiation at different frequencies.

III. PLANAR LENS

The planar lens is designed to have a radial dependence of the refractive index:

$$n(r) = \frac{1}{h} \left[\sqrt{R^2 + F^2} - \sqrt{r^2 + F^2} \right] + n(R) \quad (4)$$

where h is the thickness of the planar lens, F is the focal length and R is the maximal radius of the lens. In Eq. 1, $n(R)$ is the refractive index at the edge of the lens and can be selected arbitrarily. To minimize the losses and ensure proper mechanical rigidity of the lens, we select $n(R) = 1.2$. As for the refractive index in the center of the lens, it is inherently limited to the maximal value defined by the material refractive index (fill factor of 0, $n(0) = n_m$).

We designed and fabricated a planar lens of focal length of 15 cm with a maximal radius of 25 mm (Fig. 2a). In Fig.

2b we present an image of the THz beam at 200 GHz without the planar lens (reference). With the planar lens, the beam is correctly focused at the focal length (Fig. 2c). Cross-sections of the intensity of the THz beam at the position of the focal length with and without the planar lens are presented in Fig. 2d. The full width-half maximum without and with the planar lens are respectively 11.3 mm and 5.7 mm.

III. ORBITAL ANGULAR MOMENTUM PHASE PLATE

In the planar OAM phase plate, the refractive index varies as a function of the angle:

$$n(\theta) = \frac{\lambda m \theta}{h 2\pi} + n(0) \quad (5)$$

where λ is the wavelength, h is the thickness of the phase plate, m is the topological charge of the OAM state and $n(0)$ is the refractive index at the polar origin ($n(0) = 1.2$).

We design and fabricate an OAM phase plate with a topological charge of $m = 1$ for a frequency of 0.14 THz (Fig. 3a). The planar phase front of the THz beam is transformed to a helical phase front by the OAM plate as shown in Fig. 3b. Next, we use THz-TDS imaging to image both the amplitude and the phase of THz beam. The reference beam without the OAM phase plate show a Gaussian-like amplitude distribution (Fig. 3c) and a planar phase front (Fig. 3d). When placing the OAM phase plate, the amplitude is shaped as a donut (Fig. 3e) and the phase varies azimuthally from $-\pi$ to $+\pi$ (Fig. 3f), which are characteristic of an OAM beam with $m = 1$.

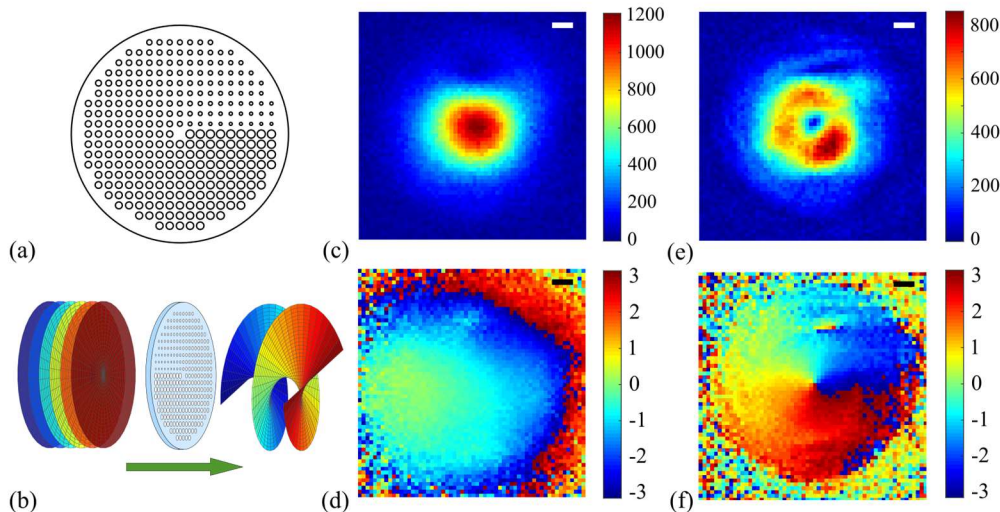


Fig. 3. (a) Design of the OAM phase plate with the diameter of the holes varying as a function of the angle following Eq. 3. (b) Schematic of the transformation of a planar phase to a helical phase with the planar OAM phase plate. (c) Amplitude and (d) phase of the 0.14-THz beam without the phase plate (reference). (e) Amplitude and (f) phase of the 0.14-THz beam with the OAM phase plate.

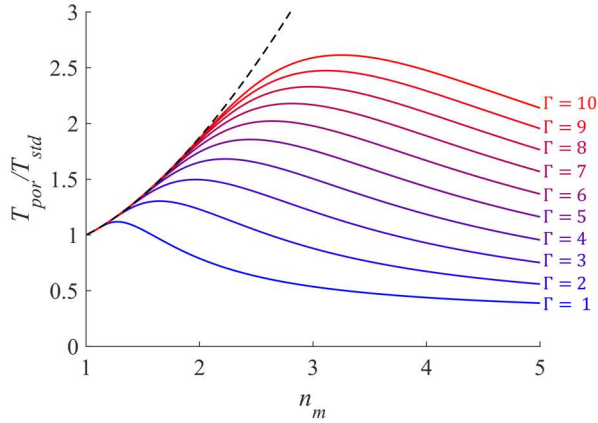


Fig. 4 Transmission ratios as a function of the material refractive index n_m for different values of Γ as described by Eq. (6). When the material has very high losses ($\Gamma \rightarrow \infty$), the ratio tends to the asymptotic value defined in Eq (7) (black dotted line).

IV. COMPARISON OF THE LOSSES OF POROUS COMPONENTS AND COMPONENTS WITH VARIABLE THICKNESSES

When comparing the transmission through porous components (T_{por}) and standard components with variable thickness (T_{std}), we can show that

$$\frac{T_{por}}{T_{std}} = \frac{\frac{n_m^4 - 1}{4n_m} \left[1 - \exp\left(-\Gamma \frac{4n_m}{n_m^4 - 1}\right) \right]}{(n_m - 1) \left[1 - \exp\left(-\Gamma \frac{1}{n_m - 1}\right) \right]} \quad (6)$$

where $\Gamma = \alpha_m R^2 / 2F$ for the lens and $\Gamma = \alpha_m m \lambda$ for the OAM phase plate. In Fig. 4, we plot several ratios as a function of n_m for different values of Γ . As we can see, the ratio is higher than 1 for certain combined values of Γ and n_m . In particular, if the material is very lossy ($\alpha_m \rightarrow \infty, \Gamma \rightarrow \infty$), the ratio is increasing superlinearly (dotted line in Fig. 4) with n_m to

$$\lim_{\Gamma \rightarrow \infty} \frac{T_{por}^{lens}}{T_{std}^{lens}} = \frac{n_m^4 - 1}{4n_m(n_m - 1)} \quad (7)$$

VII. CONCLUSION

In conclusion, we have designed, fabricated and characterized planar components for THz beam forming. Using artificial holes in a dielectric media, we created

gradient refractive index distribution by varying the hole diameters. We then fabricated a planar lens and an OAM phase plate and we have observed that both operates properly as intended. Finally, we demonstrated theoretically that both devices have larger transmission than their variable thickness counterparts. This work can have applications in low-loss THz wireless communications.

REFERENCES

- [1] I. F. Akyildiz, J. M. Jornet, C. Han, "Terahertz band: Next frontier for wireless communications," *Phys. Commun.*, vol. 12, pp. 16-32, September 2014.
- [2] T. Nagatsuma, G. Ducournau, and C. C. Renaud, "Advances in terahertz communications accelerated by photonics," *Nat. Photonics*, vol. 10, no. 6, pp. 371-379, 2016.
- [3] H. Shams, and A. Seeds, "Photonics, Fiber and THz wireless communications," *Opt. Photonics News*, vol. 28, no. 3, pp. 24-31, 2017.
- [4] D. Headland, Y. Monnai, D. Abbott, C. Fumeaux, and W. Withayachumnakul "Tutorial: Terahertz beamforming, from concepts to realizations," *APL Photonics*, vol. 3, no. 5 p. 051101, January 2018.
- [5] W. Volckaerts, N. Van Thienen, and P. Reynaert, "10.2 An FSK plastic waveguide communication link in 40nm CMOS," in *SolidState Circuits Conference-(ISSCC)*, 2015 IEEE International, 2015, pp. 1-3: IEEE.
- [6] B. Yu et al., "Ortho-Mode Sub-THz Interconnect Channel for Planar Chip-to-Chip Communications," *IEEE Transactions on Microwave Theory and Techniques*, vol. 66, no. 4, pp. 1864-1873, 2018
- [7] A. Hassani, A. Dupuis, and M. Skorobogatiy "Porous polymer fibers for low-loss terahertz guiding," *Opt. Express*, vol. 16, no. 9, pp. 6340-6351, April 2008.
- [8] S.-G. Park, K. Lee, D. Han, J. Ahn, and K.-H. Jeong, "Subwavelength silicon through-hole arrays as an all-dielectric broadband terahertz gradient index metamaterial," *Appl. Phys. Lett.*, vol. 105, no. 9, p. 091101, September 2014.
- [9] J. Wang, J.-Y. Yang, I. M. Fazal, N. Ahmed, Y. Yan, H. Huang, Y. Ren, Y. Yue, S. Dolinar, M. Tur, and A. E. Willner, "Terabit free-space data transmission employing orbital angular momentum multiplexing," *Nat. Photonics*, vol. 6, no. 7, pp. 488-496, July 2012.
- [10] M. Skorobogatiy, *Nanostructured and subwavelength waveguides*, 2012.
- [11] H. Guerbouka, K. Nallappan, and M. Skorobogatiy, "Towards real-time terahertz imaging," *Advances in Optics and Photonics*, vol. 10, no. 4, 2018.
- [12] H. Guerboukha, K. Nallappan, and M. Skorobogatiy, "Exploiting k-space/frequency duality toward real-time terahertz imaging," *Optica*, vol. 5, no. 2, pp. 109-116, January 2018.